European Conference on Computational Fluid Dynamics
ECCOMAS CFD 2006
P. Wesseling, E. Oñate and J. Périaux (Eds)
© TU Delft, The Netherlands, 2006

SYMMETRY-PRESERVING DISCRETIZATIONS OF THE INCOMPRESSIBLE NAVIER-STOKES EQUATIONS

R.W.C.P. Verstappen and A.E.P. Veldman

Institute of Mathematics and Computing Science, University of Groningen
P.O. Box 800, 9700 AV Groningen, The Netherlands
E-mail: R.W.C.P.Verstappen@rug.nl and veldman@math.rug.nl

Key words: Higher-order, finite-volume discretization, symmetry and conservation, stability, turbulent channel flow

Abstract. *We propose to discretize the convective and diffusive operators in the (incompressible) Navier-Stokes equations in such a manner that their symmetries are preserved. The resulting spatial discretization inherits all symmetry-related conservation and stability properties from the continuous formulation. In particularly, a symmetry-preserving discretization is unconditionally stable, and conserves the energy in the absense of viscous dissipation. In this paper, a fourth-order, symmetry-preserving discretization method is described and tested successfully for direct numerical simulation of turbulent channel flow ($Re_\tau = 180$).*

1 SYMMETRY AND CONSERVATION

The Navier-Stokes equations provide an appropriate model for turbulent flow. In the absence of compressibility ($\nabla \cdot u = 0$), the equations are

$$\partial_t u + (u \cdot \nabla)u + \nu \Delta u + \nabla p = 0, \tag{1}$$

where u denotes the instantaneous fluid velocity field, p stands for the pressure, and ν is the viscosity. Turbulence is basically the combination of nonlinear transport and dissipation of energy. Very crudely put, energy is convected from the main flow into the large eddies, and from them into the next smaller eddies, and so on until it reaches the smallest scales of motion, where viscous dissipation is the most effective. In the absence of external sources (such as body or boundary forces), the rate of change of the total energy is neither influenced by convective transport nor by pressure differences; it is solely determined by viscous dissipation. This basic property can readily be deduced from the symmetries of the differential operators in (1). To that end, we consider the evolution of the energy. In terms of the usual scalar product $(u, v) = \int_V u \cdot v dx$, the energy of a fluid with velocity u and occupying a region V is given by $|u|^2 = (u, u)$. Differentiating

(u, u) with respect to time and rewriting $\partial_t u$ with the help of (1) gives

$$\frac{\mathrm{d}}{\mathrm{d}t}|u|^2 = -\left((u\cdot\nabla)u, u\right) - \left(u, (u\cdot\nabla)u\right) - \nu\left(\Delta u, u\right) - \nu\left(u, \Delta u\right) - \left(\nabla p, u\right) - \left(u, \nabla p\right).$$

Here, the convective contributions cancel, because the trilinear form $((u\cdot\nabla)v, w)$ satisfies

$$\left((u\cdot\nabla)v, w\right) = -\left(v, (u\cdot\nabla)w\right), \tag{2}$$

or, stated otherwise, because the convective operator $(u\cdot\nabla)$ is skew symmetric:

$$(u\cdot\nabla) + (u\cdot\nabla)^* = 0. \tag{3}$$

The proof of (2) uses the identity

$$\nabla\cdot(fu) = f\nabla\cdot u + \nabla f\cdot u, \tag{4}$$

which holds for any (differentiable) scalar f and vector field u. Taking $f = v\cdot w$, $\nabla\cdot u = 0$ and applying Gauß's Divergence Theorem gives

$$\begin{aligned}\int_{\partial V}(v\cdot w)(u\cdot n)ds &= \int_V \nabla\cdot\left((v\cdot w)u\right)dV = \int_V \nabla(v\cdot w)\cdot u dV\\ &= \int_V (u\cdot\nabla)v\cdot w dV + \int_V (u\cdot\nabla)w\cdot v dV,\end{aligned}$$

which shows that (2) holds if the boundary term vanishes, *e.g.*, if the normal velocity $u\cdot n$ vanishes at the boundary ∂V, or if $v\cdot w$ vanishes, or if periodic boundary conditions apply. Likewise, by setting $f = p$ in (4) and applying Gauß's Divergence Theorem again, we obtain that $(\nabla p, u) = 0$ if $u\cdot n = 0$ at the boundary. Therefore, the pressure does not contribute to the energetics (in the absence of in-/outflow boundaries). Thus after some algebra, the energy equation reduces to

$$\frac{\mathrm{d}}{\mathrm{d}t}\tfrac{1}{2}|u|^2 = -\nu|\nabla u|^2 \tag{5}$$

When the Navier-Stokes equations are discretized in space, the discrete energy also evolves according to Eq. (5) with u replaced by the discrete velocity, and ∇ by its discrete approximation, provided the underlying symmetries are preserved. That is, a symmetry-preserving discretization of the incompressible Navier-Stokes equations conserves the discrete energy exactly in case $\nu = 0$, and decreases the discrete energy for $\nu > 0$ (in the absence of external sources).

1.1 1D example

To illustrate the need to preserve the skew-symmetry (3), we consider the linear convection equation (in one spatial dimension)

$$\partial_t u + \partial_x u = 0. \tag{6}$$

The spatial discretization problem reads: given three values of u, say $u_{i-1} = u(x_{i-1})$, $u_i = u(x_i)$ and $u_{i+1} = u(x_{i+1})$ with $x_{i-1} < x_i < x_{i+1}$, find an approximation of $\partial_x u$ in x_i. Traditionally, the approximation is constructed to minimize the local truncation error, which results in

$$\partial_x u(x_i) \approx \frac{r_i u_{i+1} - (r_i - r_i^{-1})u_i - r_i^{-1} u_{i-1}}{x_{i+1} - x_{i-1}}, \tag{7}$$

where $r_i = (x_i - x_{i-1})/(x_{i+1} - x_i)$. This approximation may also be derived by constructing a parabola through the three given data points and differentiating that parabola at $x = x_i$. To analyze the energetics of the semi-discrete system given by Eqs. (6)-(7), we write it in a finite-volume fashion,

$$\boldsymbol{\Omega} \frac{\mathrm{d}\boldsymbol{u}_h}{\mathrm{d}t} + \boldsymbol{C}\boldsymbol{u}_h = \boldsymbol{0}, \tag{8}$$

where the semi-discrete velocities u_i constitute the vector $\boldsymbol{u}_h$, the diagonal matrix $\boldsymbol{\Omega}$ is built of the control volumes $\frac{1}{2}(x_{i+1} - x_{i-1})$ and tridiagonal matrix $\boldsymbol{C}$ contains the coefficients of the convective discretization. The discrete energy $||\boldsymbol{u}_h||^2 = \boldsymbol{u}_h^* \boldsymbol{\Omega} \boldsymbol{u}_h$ of any solution of the dynamical system (8) is conserved if and only if the right hand-side of

$$\frac{\mathrm{d}}{\mathrm{d}t}||\boldsymbol{u}_h||^2 = \frac{\mathrm{d}}{\mathrm{d}t}\left(\boldsymbol{u}_h^* \boldsymbol{\Omega} \boldsymbol{u}_h\right) \overset{(8)}{=} -\boldsymbol{u}_h^* \left(\boldsymbol{C} + \boldsymbol{C}^*\right) \boldsymbol{u}_h$$

vanishes. This conservation property holds (for any $\boldsymbol{u}_h$) if and only if the coefficient matrix $\boldsymbol{C}$ is skew symmetric. However, we see immediately that (7) leads to a coefficient matrix $\boldsymbol{C}$ with nonzero diagonal entries for nonuniform grids ($r_i \neq 1$). Hence, if the local truncation error is minimized, the skew symmetry of the convective operator is lost on nonuniform grids. This forms our main motivation to consider the skew-symmetric discretization

$$\partial_x u(x_i) \approx \frac{u_{i+1} - u_{i-1}}{x_{i+1} - x_{i-1}}, \tag{9}$$

instead of (7). On uniform grids ($r_i = 1$) we obtain, of course, the usual second-order discretization (7), but on nonuniform grids (7) and (9) differ. The two ways of discretization are illustrated in Figure 1.

The symmetry-preserving discretization (9) may be derived by means of the coordinate transformation $x = x(\xi)$, which maps the nonuniform grid in x onto a uniform grid in ξ. Prior to discretization, we rewrite the (partial) derivative of u with respect to x as a quotient of derivatives with respect to ξ

$$\frac{\partial u}{\partial x} = \frac{\partial u}{\partial \xi}\frac{\mathrm{d}\xi}{\mathrm{d}x} = \frac{\partial u}{\partial \xi} \Big/ \frac{\mathrm{d}x}{\mathrm{d}\xi}.$$

The two ξ-derivatives in the right-hand side are discretized on the ξ-grid, which has a uniform spacing denoted by h. Neglecting second-order terms in

$$\frac{\partial u}{\partial \xi}(\xi_i) = \frac{u_{i+1} - u_{i-1}}{2h} + O(h^2),$$

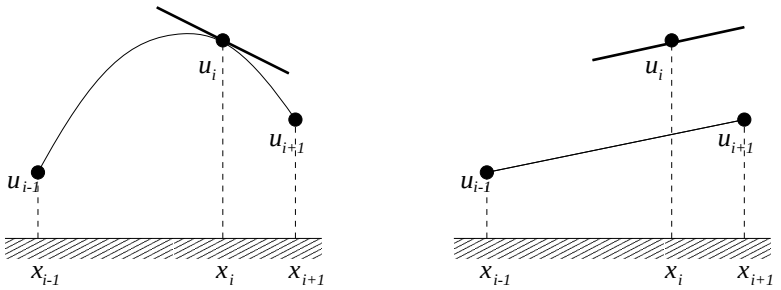

Figure 1: Two ways of approximating $\partial_x u$. In the left-hand figure the derivative is approximated by means of a Lagrangian interpolation, that is by Eq. (7). In the right-hand figure the symmetry-preserving discretization (9) is applied.

and

$$\frac{\mathrm{d}x}{\mathrm{d}\xi}(\xi_i) = \frac{x_{i+1} - x_{i-1}}{2h} + O(h^2),$$

gives the approximation (9). This derivation illustrates the second-order accuracy of the skew-symmetric discretization (9) on nonuniform grids, see also [1]-[2]. Therewith it founds our choice for the skew-symmetric discretization (9).

1.2 Navier-Stokes equations

The example given above illustrates the importance of the skew symmetry of the discrete convective operator. With this example in mind, we have developed a symmetry-preserving discretization method for the incompressible Navier-Stokes equations. In matrix-vector notation, the spatial discretization reads

$$\boldsymbol{\Omega}\frac{\mathrm{d}\boldsymbol{u}_h}{\mathrm{d}t} + \boldsymbol{C}(\boldsymbol{u}_h)\boldsymbol{u}_h + \boldsymbol{D}\boldsymbol{u}_h + \boldsymbol{M}^*\boldsymbol{p}_h = \boldsymbol{0} \qquad \boldsymbol{M}\boldsymbol{u}_h = \boldsymbol{0}, \tag{10}$$

where $\boldsymbol{p}_h$ denotes the discrete pressure, $\boldsymbol{\Omega}$ is a (positive-definite) diagonal matrix representing the sizes of the control volumes and $\boldsymbol{M}$ is the coefficient matrix of the discretization of the integral form of the law of conservation of mass. The matrices $\boldsymbol{C}(\boldsymbol{u}_h)$ and $\boldsymbol{D}$ represent the convective and diffusive discretization, respectively.

If the convective coefficient matrix $\boldsymbol{C}(\boldsymbol{u}_h)$ is skew symmetric like the convective operator $(\boldsymbol{u}\cdot\nabla)$,

$$\boldsymbol{C}\left(\boldsymbol{u}_h\right) + \boldsymbol{C}\left(\boldsymbol{u}_h\right)^* = \boldsymbol{0}, \tag{11}$$

compare (2) with (11), the evolution of the energy of any solution of (10) is governed by

$$\begin{aligned}\frac{\mathrm{d}}{\mathrm{d}t}(\boldsymbol{u}_h^*\boldsymbol{\Omega}\boldsymbol{u}_h) &\overset{(10)}{=} -\boldsymbol{u}_h^*(\boldsymbol{C}\left(\boldsymbol{u}_h\right) + \boldsymbol{C}\left(\boldsymbol{u}_h\right)^*)\boldsymbol{u}_h - \boldsymbol{u}_h^*(\boldsymbol{D}+\boldsymbol{D}^*)\boldsymbol{u}_h \\ &\overset{(11)}{=} -\boldsymbol{u}_h^*(\boldsymbol{D}+\boldsymbol{D}^*)\boldsymbol{u}_h.\end{aligned}$$

Here, the right-hand side is negative for any $\boldsymbol{u}_h$ (not in the null space of $\boldsymbol{D}+\boldsymbol{D}^*$) if the matrix $\boldsymbol{D}+\boldsymbol{D}^*$ is positive definite, like the continuous, diffusive operator $-\nu\Delta$. Note that the discrete pressure does not contribute to the evolution of the discrete energy since $(\boldsymbol{M}^*\boldsymbol{p}_h)^*\boldsymbol{u}_h = \boldsymbol{p}_h^*\boldsymbol{M}\boldsymbol{u}_h = 0$.

In conclusion, the rate of change of the discrete energy is not influenced by convective transport if and only if the discrete convective operator satisfies (11). Then, the energy decreases in time if the diffusive operator $\boldsymbol{D}$ is positive definite, and the matrix $\boldsymbol{C}(\boldsymbol{u}_h)+\boldsymbol{D}$ is regular, because all eigenvalues lie in the stable half-plane, *i.e.*, a solution of (10) can be obtained on any grid.

Both stability and conservation properties have a long standing in the analysis of discretization methods for the (incompressible) Navier-Stokes equations. Recently, conservation properties are also pursued by other researchers, see [3]-[5], for example. The current issue is how to construct a fully-conservative, fourth-order scheme on nonuniform grids.

2 SYMMETRY-PRESERVING DISCRETIZATION

In the previous section, we saw that conservation properties and stability are directly related to the symmetry of the discrete operators in Eq. (10). In this section, the symmetry-preserving discretization is worked out in detail on staggered, nonuniform grids (in two spatial dimensions to limit the length of the presentation).

2.1 Convective discretization

To prepare for the skew-symmetric discretization of the convective derivative, we recall the transport theorem: for any function f, we have

$$\frac{d}{dt}\int_\Omega f dV = \int_\Omega \frac{\partial f}{\partial t} dV + \int_{\partial\Omega} f\boldsymbol{u}\cdot\boldsymbol{n} dS, \tag{12}$$

where Ω is an arbitrary part of the fluid (at time t). The unit vector $\boldsymbol{n}$ denotes the outward normal on the surface $\partial\Omega$ of Ω. The function f can have several meanings depending on what is transported. Taking f equal to the mass density gives the law of conservation of mass. For an incompressible fluid, it states that the net mass flux through the faces of any grid cell $[x_{i-1},x_i]\times[y_{j-1},y_j]$ is zero,

$$\overline{u}_{i,j} + \overline{v}_{i,j} - \overline{u}_{i-1,j} - \overline{v}_{i,j-1} = 0, \tag{13}$$

where the mass fluxes through the faces are defined by

$$\overline{u}_{i,j} = \int_{y_{j-1}}^{y_j} u(x_i,y,t)dy \quad\text{and}\quad \overline{v}_{i,j} = \int_{x_{i-1}}^{x_i} v(x,y_j,t)dx. \tag{14}$$

Note that the combination (13)-(14) does not yet contain a discretization error.

The transport of momentum of a region Ω in an incompressible fluid is obtained if f in Eq. (12) is replaced by the momentum. As mass and momentum are transported at equal velocity, we will use the (14) for the transport velocity. Thus, the momentum flux through a surface S is approximated by

$$\int_S u\boldsymbol{u}\cdot\boldsymbol{n}dS \approx u_S \int_S \boldsymbol{u}\cdot\boldsymbol{n}dS,$$

where u_S denotes a characteristic value of u at the surface S. At this stage, the integral in the right-hand side (that is the mass flux through S) is not approximated. The control volume $\Omega_{i+1/2,j}$ for the component $u_{i,j}$ of the discrete velocity is defined as in the Marker-and-Cell method [6]), that is $\Omega_{i+1/2,j} = [x_{i-1/2}, x_{i+1/2}] \times [y_{j-1}, y_j]$; see Figure 2.

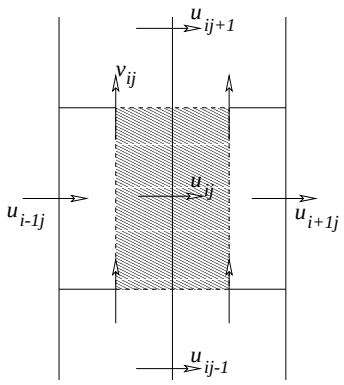

Figure 2: The control volume $\Omega_{i+1/2,j}$ for the discrete, horizontal velocity $u_{i,j}$.

The transport of momentum through the faces of the control volume $\Omega_{i+1/2,j}$ becomes approximately

$$\begin{aligned} |\Omega_{i+1/2,j}|\frac{\mathrm{d}u_{i,j}}{\mathrm{d}t} \quad &+ \quad u_{i+1/2,j}\overline{u}_{i+1/2,j} + u_{i,j+1/2}\overline{v}_{i+1/2,j} \\ &- \quad u_{i-1/2,j}\overline{u}_{i-1/2,j} - u_{i,j-1/2}\overline{v}_{i+1/2,j-1}. \end{aligned} \tag{15}$$

The first term in (15) represents the discretization of the volume integral in the right-hand side of (12); the other terms form the approximation of the surface integral in (12) with $f = u$. The non-integer indices in (15) refer to the faces of the control cell for $u_{i,j}$. For example, $u_{i-1/2,j}$ stands for a characteristic u-velocity at the interface of $\Omega_{i-1/2,j}$ and $\Omega_{i+1/2,j}$ and $\overline{v}_{i+1/2,j}$ denotes the (exact) mass flux through the common boundary of the control volumes for $u_{i,j}$ and $u_{i,j+1}$, etc.

The velocity at a control face is approximated by the average of the velocity at both sides of it:

$$u_{i+1/2,j} = \tfrac{1}{2}(u_{i+1,j} + u_{i,j}) \quad \text{and} \quad u_{i,j+1/2} = \tfrac{1}{2}(u_{i,j+1} + u_{i,j}). \tag{16}$$

In addition to the set of equations for the u-component of the velocity $\boldsymbol{u} = (u, v)$, there is an analogous set for the v-component. We conceive the combination (15)-(16) as an expression for the velocities, where the mass fluxes form the coefficients. In matrix-vector notation, we can write (15)-(16), together with an analogous set for the v-component, as

$$\boldsymbol{\Omega}\frac{\mathrm{d}\boldsymbol{u}_h}{\mathrm{d}t} + \boldsymbol{C}(\bar{\boldsymbol{u}})\boldsymbol{u}_h, \tag{17}$$

where the coefficient matrix $\boldsymbol{C}(\bar{\boldsymbol{u}})$ depends on the mass fluxes through the control faces. Note that we make liberal use of its name: so far $\boldsymbol{C}$ was viewed as a function of $\boldsymbol{u}_h$, whereas $\boldsymbol{C}$ is a function of exact mass fluxes here.

In the introductory section, we saw that (for $\boldsymbol{D} = \boldsymbol{0}$) the spatial discretization (10) conserves the energy $\boldsymbol{u}_h^*\boldsymbol{\Omega}\boldsymbol{u}_h$ if and only if the convective coefficient matrix $\boldsymbol{C}\,(\bar{\boldsymbol{u}})$ is skew symmetric. The matrix $\boldsymbol{C}\,(\bar{\boldsymbol{u}}) - \mathrm{diag}(\boldsymbol{C}\,(\bar{\boldsymbol{u}}))$ is skew symmetric if and only if the weights in the interpolation of u (and v) to the control faces are constant, as in Eq. (16). Therefore we use (16) also on nonuniform grids. To make $\boldsymbol{C}\,(\bar{\boldsymbol{u}})$ skew symmetric, the interpolation rule for $\overline{u}$ and $\overline{v}$ is determined by the requirement that the diagonal of $\boldsymbol{C}\,(\bar{\boldsymbol{u}})$ has to be zero. By substituting the interpolation (16) into (15) we obtain the diagonal coefficient

$$\tfrac{1}{2}\left(\overline{u}_{i+1/2,j} + \overline{v}_{i+1/2,j} - \overline{u}_{i-1/2,j} - \overline{v}_{i+1/2,j-1}\right).$$

This expression is zero if the mass is conserved in the grid cells and the mass fluxes in (15) are interpolated to the control faces with weights one half:

$$\overline{u}_{i+1/2,j} = \tfrac{1}{2}(\overline{u}_{i+1,j} + \overline{u}_{i,j}) \quad \text{and} \quad \overline{v}_{i+1/2,j} = \tfrac{1}{2}(\overline{v}_{i+1,j} + \overline{v}_{i,j}). \tag{18}$$

2.2 The discrete divergence and gradient

Obviously, the mass flux $\bar{\boldsymbol{u}}$ needs to be expressed in terms of the discrete velocity vector $\boldsymbol{u}_h$ to close the discretization. The coefficient matrix becomes a function of the discrete velocity then: $\boldsymbol{C}(\boldsymbol{u}_h) = \boldsymbol{C}(\bar{\boldsymbol{u}}(\boldsymbol{u}_h))$. The matrix $\boldsymbol{C}(\boldsymbol{u}_h)$ is skew symmetric for any relation between $\bar{\boldsymbol{u}}$ and $\boldsymbol{u}_h$. We take $\overline{u}_{i,j} = (y_j - y_{j-1})u_{i,j}$ and $\overline{v}_{i,j} = (x_i - x_{i-1})v_{i,j}$. Substituting these approximations into Eq. (13) yields the discrete continuity constraint, which confines the discrete velocity to $\boldsymbol{M}\boldsymbol{u}_h = \boldsymbol{0}$.

The discrete gradient matrix, describing the integration of the pressure gradient over the control volumes $\boldsymbol{\Omega}$, is given by $\boldsymbol{M}^*$. Consequently, the pressure term in Eq. (10) does not contribute to the evolution of the discrete energy. To make the velocity field divergence-free, the pressure is computed from a Poisson equation, where the discrete Laplacian $-\boldsymbol{M}\boldsymbol{\Omega}^{-1}\boldsymbol{M}^*$ is symmetric and negative definite.

2.3 Diffusive discretization

The method for discretizing the Laplacian in the Poisson equation for the pressure is also applied to discretize the diffusive term $\nu\Delta u$ in Eq.(1). In short, the diffusive operator

is viewed as the product of a divergence and gradient. The divergence is discretized and the discrete gradient becomes the transpose of the discrete divergence (multiplied by a diagonal scaling). Unfortunately, we can not re-use the approximation $\boldsymbol{M}\boldsymbol{\Omega}^{-1}\boldsymbol{M}^*$, since, due to staggering of the grid, the control volumes for u and v differ from the grid cells on which coefficient matrix $\boldsymbol{M}$ is based. Therefore, we have to introduce the matrices $\boldsymbol{M}_u$ and $\boldsymbol{M}_v$. They stand for the discrete integration of the divergence over the control volumes for u and v, respectively. Thus, the discrete diffusive operator in (10) becomes symmetric, positive definite:

$$\boldsymbol{D} = \nu \, \mathrm{diag}\left(\boldsymbol{M}_u\boldsymbol{\Omega}_u^{-1}\boldsymbol{M}_u^*, \boldsymbol{M}_v\boldsymbol{\Omega}_v^{-1}\boldsymbol{M}_v^*\right). \tag{19}$$

2.4 Fourth-order discretization

To turn Eq. (15) into a higher-order approximation, we write down the transport of momentum of a region $\Omega^{(3)}_{i+1/2,j} = [x_{i-3/2}, x_{i+3/2}] \times [y_{j-2}, y_{j+1}]$. Here, it may be noted that we can not blow up the 'original' volumes $\Omega_{i+1/2,j}$ by a factor of two (in all directions) since our grid is not collocated. On a staggered grid, three times larger volumes are the smallest ones possible for which the same discretization rule can be applied as for the 'original' volumes. This yields

$$\begin{aligned} |\Omega^{(3)}_{i+1/2,j}|\frac{\mathrm{d}u_{i,j}}{\mathrm{d}t} &+ \bar{\bar{u}}_{i+3/2,j}u_{i+3/2,j} + \bar{\bar{v}}_{i+1/2,j+1}u_{i,j+3/2} \\ &- \bar{\bar{u}}_{i-3/2,j}u_{i-3/2,j} - \bar{\bar{v}}_{i+1/2,j-2}u_{i,j-3/2}, \end{aligned} \tag{20}$$

where the mass fluxes

$$\bar{\bar{u}}_{i,j} = \int_{y_{j-2}}^{y_{j+1}} u(x_i, y, t)dy \quad \text{and} \quad \bar{\bar{v}}_{i,j} = \int_{x_{i-2}}^{x_{i+1}} v(x, y_j, t)dy \tag{21}$$

satisfy

$$\bar{\bar{u}}_{i+1,j} + \bar{\bar{v}}_{i,j+1} - \bar{\bar{u}}_{i-2,j} - \bar{\bar{v}}_{i,j-2} = 0. \tag{22}$$

The velocities at the control faces of the large volumes are interpolated to the control faces in a way similar to that given by Eq. (16):

$$u_{i+3/2,j} = \tfrac{1}{2}(u_{i+3,j} + u_{i,j}) \quad \text{and} \quad u_{i,j+3/2} = \tfrac{1}{2}(u_{i,j+3} + u_{i,j}). \tag{23}$$

We can recapitulate the equations above (together with the analogous set for the v-component) by

$$\boldsymbol{\Omega}_3\frac{\mathrm{d}\boldsymbol{u}_h}{\mathrm{d}t} + \boldsymbol{C}_3(\bar{\bar{\boldsymbol{u}}})\boldsymbol{u}_h, \tag{24}$$

where the diagonal matrix $\boldsymbol{\Omega}_3$ represents the sizes of the large control volumes and $\boldsymbol{C}_3$ consists of flux contributions ($\bar{\bar{u}}$ and $\bar{\bar{v}}$) through the faces of these volumes.

On a uniform grid the local truncation errors in Eqs. (17) and (24) are of the order $2 + d$, where $d = 2$ in two spatial dimensions and $d = 3$ in 3D. The leading term in the

discretization error may be removed through a Richardson extrapolation (just like in [7]). This leads to the fourth-order approximation

$$\left(3^{2+d}\boldsymbol{\Omega} - \boldsymbol{\Omega}_3\right) \frac{\mathrm{d}\boldsymbol{u}_h}{\mathrm{d}t} + \left(3^{2+d}\boldsymbol{C}(\bar{\boldsymbol{u}}) - \boldsymbol{C}_3(\bar{\bar{\boldsymbol{u}}})\right) \boldsymbol{u}_h.$$

The fourth-order approximation of the law of conservation of mass becomes

$$(3^{2+d}\boldsymbol{M} - \boldsymbol{M}_3)\boldsymbol{u}_h = \boldsymbol{0}, \tag{25}$$

where $\boldsymbol{M}_3\boldsymbol{u}_h = \boldsymbol{0}$ represents the discretization of (22) in matrix-vector notation.

Except for the diagonal, the linear combination $3^{2+d}\boldsymbol{C}(\bar{\boldsymbol{u}}) - \boldsymbol{C}_3(\bar{\bar{\boldsymbol{u}}})$ is skew-symmetric. In order to maintain this property on nonuniform grids, the weights 3^{2+d} and -1 are to be used on nonuniform grids too. The $\bar{\boldsymbol{u}}$'s and $\bar{\bar{\boldsymbol{u}}}$'s are to be interpolated to the control faces in such a manner that the diagonal of resulting convective matrix $3^{2+d}\boldsymbol{C}(\bar{\boldsymbol{u}}) - \boldsymbol{C}_3(\bar{\bar{\boldsymbol{u}}})$ vanishes for all discrete velocities satisfying (25). To achieve this, we may interpolate $\bar{u}_{i+1/2,j}$ in the following manner

$$\bar{u}_{i+1/2,j} = \tfrac{1}{2}\alpha(\bar{u}_{i+1,j} + \bar{u}_{i,j}) + \tfrac{1}{2}(1-\alpha)(\bar{u}_{i+2,j} + \bar{u}_{i-1,j}), \tag{26}$$

where α is a constant, and interpolate $\bar{v}_{i+1/2,j}$, $\bar{\bar{u}}_{i+1/2,j}$ and $\bar{\bar{v}}_{i+1/2,j}$ likewise. As in Morinishi *et al.* [3] we take $\alpha = 9/8$ because all interpolations are fourth-order accurate then (on a uniform grid).

Finally, it may be noted that a fourth-order, positive-definite discretization of diffusion can be constructed in the same vein, see [8] for details.

3 RESULTS FOR TURBULENT CHANNEL FLOW

The symmetry-preserving discretization is tested for turbulent channel flow. The Reynolds number is $Re_\tau = 180$ (based on the channel half-width and the wall-shear velocity). This flow forms a prototype for near-wall turbulence. As usual, the flow is assumed to be periodic in the stream- and spanwise direction. Consequently, the computational domain may be confined to a channel unit of dimension $2\pi \times 1 \times \pi$, where the width of the channel is normalized. The computational grid consists of 64 (uniformly distributed) streamwise points, 32 (uniformly distributed) spanwise points and N_y wall-normal points. Fig. 3 shows a comparison of the mean velocity as obtained from our fourth-order symmetry-preserving simulation ($N_y = 64$) with those of other direct numerical simulations [9]-[10]. Here it may be stressed that the grids used by the DNS's that we compare with have about 16 times more grid points than our grid has.

To investigate the convergence of the fourth-order method upon grid refinement, we have monitored the skin friction coefficient C_f as obtained from simulations on five different grids. We will denote these grids by A, B, C, D and E. Their spacings differ only in the direction normal to the wall. They have $N_y = 128$ (grid A), $N_y = 96$ (B), $N_y = 64$ (C), $N_y = 56$ (D) and $N_y = 48$ (E) points in the wall-normal direction, respectively.

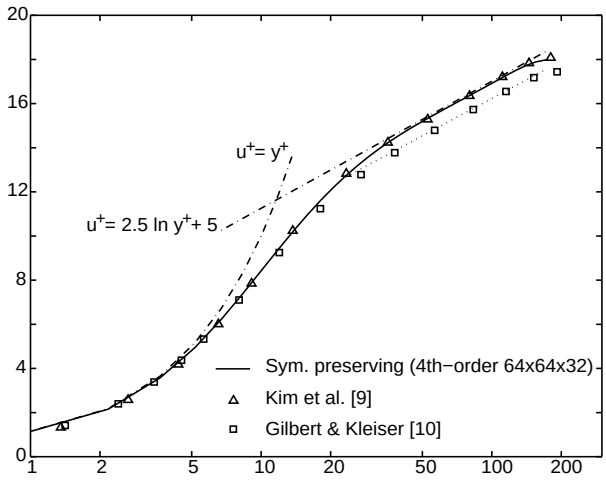

Figure 3: Comparison of the mean velocity. The dashed lines represent the law of the wall and the log law. The markers represent DNS-results that are taken from the ERCOFTAC Database.

The first (counted from the wall) grid line used for the convergence study is located at $y_1^+ \approx 0.72$ (grid A), $y_1^+ \approx 0.95$ (B), $y_1^+ \approx 1.4$ (C), $y_1^+ \approx 1.6$ (D), and $y_1^+ \approx 1.9$ (E), respectively. Figure 4 displays the skin friction coefficient C_f as function of the fourth power of the local grid spacing (measured by y_1^+). The convergence study shows that the discretization scheme is indeed fourth-order accurate, on a nonuniform mesh. This indicates that the underlying physics is resolved when 48 or more grid points are used in the wall normal direction. The straight line in Figure 4 is approximately given by $C_f = 0.00836 - 0.000004(y_1^+)^4$. The extrapolated value at the crossing with the vertical axis $y_1^+ = 0$ lies in between the C_f reported by Kim *et al.* [9] (0.00818) and Dean's correlation of $C_f = 0.073\, Re^{-1/4} = 0.00844$ [11]. Note that the extrapolation eliminates the (leading term of the) discretization error in the wall-normal direction, but not the other discretization errors in space and time.

The results for the fluctuating streamwise velocity $u_{\rm rms}$ are compared to the experimental data of Kreplin & Eckelmann [12] and to the numerical data of Kim *et al.* [9] as well as Gilbert & Kleiser [10] in Fig. 5. This comparison confirms that the fourth-order, symmetry-preserving method is more accurate than the second-order method. With 48 or more grid points in the wall normal direction, the root-mean-square of the fluctuating velocity obtained by the fourth-order method is in close agreement with the reference data. However, the turbulence intensity in the sub-layer ($0 < y^+ < 5$) predicted by the simulations is higher than that in the experiment of Kreplin & Eckelmann. According to the fourth-order simulation the root-mean-square approaches the wall like $u_{\rm rms} \approx 0.38 y^+$ ($N_y = 64$). The exact value of this slope is hard to pin-point experimentally. Hanratty *et al.* [13] have fitted experimental data of several investigators, and thus came to 0.3. Most direct numerical simulations yield higher values. Kim *et al.* [9] and Gilbert & Kleiser [10] have found slopes of 0.3637 and 0.3824 respectively, which is in close agreement with the present findings.

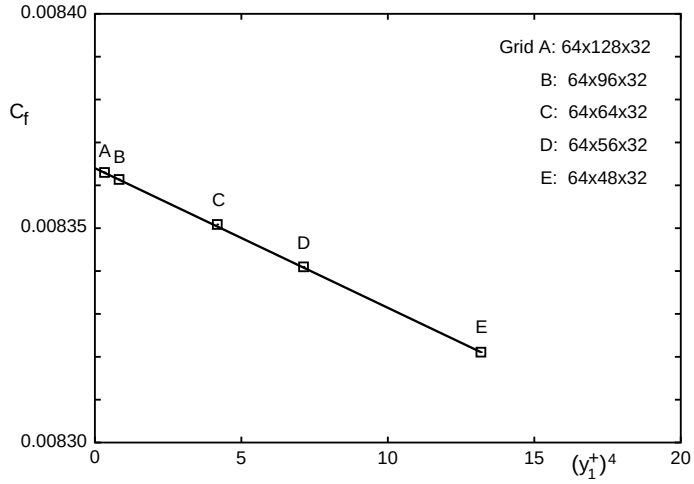

Figure 4: Convergence of the skin friction coefficient C_f upon grid refinement. The figure displays C_f versus the fourth power of the first grid point y_1^+.

REFERENCES

[1] T.A. Manteufel and A.B. White Jr. The numerical solution of second-order boundary value problems on nonuniform meshes. *Math. of Comp.*, **47**, 511–535, (1986).

[2] A.E.P. Veldman and K. Rinzema. Playing with nonuniform grids. *J. Engng. Math* **26**, 119–130, (1991).

[3] Y. Morinishi, T.S. Lund, O.V. Vasilyev and P. Moin. Fully conservative higher order finite difference schemes for incompressible flow. *J. Comp. Phys.*, **143**, 90–124, (1998).

[4] O.V. Vasilyev. High order finite difference schemes on non-uniform meshes with good conservation properties. *J. Comp. Phys.*, **157**, 746–761, (2000).

[5] F. Ducros, F. Laporte, T. Soulères, V. Guinot, P. Moinat and B. Caruelle. (2000). High-order fluxes for conservative skew-symmetric-like schemes in structured meshes: application to compressible flows. *J. Comp. Phys.*, **161**, 114–139, (2000).

[6] F.H. Harlow and J.E. Welsh. Numerical calculation of time-dependent viscous incompressible flow of fluid with free surface. *Phys. Fluids*, **8**, 2182–2189, (1965).

[7] M. Antonopoulos-Domis. Large-eddy simulation of a passive scalar in isotropic turbulence. *J. Fluid Mech.*, **104**, 55–79, (1981).

[8] R.W.C.P. Verstappen and A.E.P. Veldman. Symmetry-preserving discretization of turbulent flow. *J. Comp. Phys.*, **187**, 343–368, (2003).

[9] J. Kim, P. Moin and R. Moser. Turbulence statistics in fully developed channel flow at low Reynolds number. *J. Fluid Mech.*, **177**, 133–166,(1987).

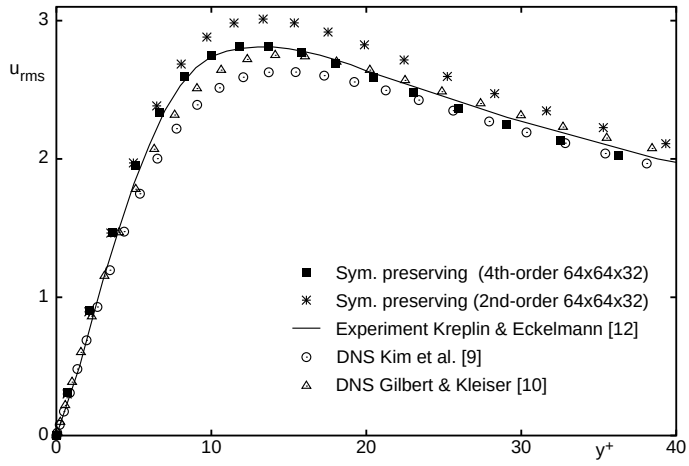

Figure 5: Comparison of the root-mean-square of the fluctuating streamwise velocity.

[10] N. Gilbert and L. Kleiser. Turbulence model testing with the aid of direct numerical simulation results. In *Proc. Turb. Shear Flows 8*, Paper 26-1, (1991).

[11] R.B. Dean. Reynolds number dependence of skin friction and other bulk flow variables in two-dimensional rectangular duct flow. *J. Fluids Engng.*, **100**, 215–223, (1978).

[12] H.P. Kreplin and H. Eckelmann. Behavior of the three fluctuating velocity components in the wall region of a turbulent channel flow. *Phys. Fluids*, **22**, 1233-1239, (1979).

[13] T.J. Hanratty, L.G. Chorn and D.T. Hatziavramidis. Turbulent fluctuations in the viscous wall region for Newtonian and drag reducing fluids. *Phys. Fluids*, **20**, S112, (1977).